Journal of Ceramic Processing Research. Vol. 24, No. 4, pp. 728~735 (2023)
(Received 5 June 2023, Received in revised form 17 July 2023, Accepted 28 July 2023)
https://doi.org/10.36410/jcpr.2023.24.4.728

JOURNAL OF
Ceramic Processing Research

Effect of La_2O_3 on the microstructure and electrical properties of ZnO linear resistors

Yajun Fu[#], Jiajia Lu[#], Jin Wang and Liangfeng Li*
School of Materials and Chemistry, Southwest University of Science and Technology, Mianyang 621010, China

ZnO-MgO-Al_2O_3-TiO_2-Y_2O_3 linear resistors with different amount of La_2O_3 were successfully prepared by the conventional solid-state sintering method. The crystalline phase composition, microstructure, and electrical properties of La_2O_3 doped ZnO linear resistors were investigated. The results show that La_2O_3 influences the lattice of ZnO and generates La-rich phase at the grain boundaries, which improves the dense density of ZnO linear resistors. The addition of La_2O_3 further affect the electrical properties of ZnO linear resistors, such as the temperature stability. The sample with 0.5 wt.% La_2O_3 show excellent electrical performance with an resistance-temperature coefficient of 0.21×10^{-3}/°C and an nonlinear coefficient of 1.05.

Keywords: ZnO linear resistor, La_2O_3, Microstructure, Electrical properties.

Introduction

As an n-type semiconductor with a wide bandgap of 3.37 eV, ZnO has been widely used in solar cells [1-3], sensors [4-6], high frequency devices [7-9], photocatalysis [10-12], varistors [13-15], linear resistors [16-18] and so on. ZnO linear resistor, which has low resistance-temperature coefficient and small nonlinear coefficient, is a kind of composite resistance material with ZnO as the host material and oxides such as MgO, Al_2O_3, TiO_2, and SiO_2 as the additives [17-22]. Compared with traditional metal and carbon based resistors, ZnO linear resistors have large flow density, adjustable resistivity, better stability, and excellent resistance-temperature characteristic [22-24]. Therefore, ZnO linear resistors have been widely used in high energy areas such as neutral grounding resistors and circuit breakers [16].

The addition of oxides is one of the most efficient way to improve the performance of ZnO linear resistances. Fe_2O_3 can be used as a donor dopant to reduce the barrier height of the grain boundary and improve the linear current-voltage (*I*-*V*) characteristic of ZnO linear resistors [21]. The addition of NiO into ZnO linear resistors improves the microstructure uniformity, energy density, and resistance-temperature characteristic [25]. CaO doping can limit the grain size of ZnO linear resistors, and then improve the electrical properties, including decrease the grain boundary barrier height and nonlinear coefficient, as well as optimize the resistance-temperature coefficient [26]. The doping of Sc_2O_3 enhances the linear characteristics of ZnO linear resistor, and further affects its dielectric properties [17].

In addition to the type of the doped oxides, the reactions of the doped oxides and ZnO also influence the performance of ZnO linear resistors [20, 27, 28]. The added oxides react with ZnO to produce spinel during the sintering process, which can modulate the resistance of the linear resistor and improve its resistance-temperature characteristic [22, 23]. As a rare earth oxide, La_2O_3 may react with ZnO, that is, the La^{3+} plays a donor dopant to substitute Zn^{2+} in the ZnO grains and create lattice defects [29]. On the other hand, the addition of La_2O_3 is likely to lead to La-rich phase in the ZnO linear resistors. Thus, the barrier height at the grain boundary and the resistance characteristic of ZnO linear resistor may be modulated by the doping amount of La_2O_3. Recent report on La_2O_3 doped ZnO linear resistors indicates that La_2O_3 doping can promote the performance of ZnO linear resistors and could enables its application in high-frequency electric field [22]. Further investigating the effect of La_2O_3 doping on ZnO linear resistors helps to better understand the mecha nism of the promoted electrical performance and further modulate its electrical properties. In our work, ZnO-MgO-Al_2O_3-TiO_2-Y_2O_3 linear resistors with different addition amounts of La_2O_3 were prepared via conventional solid-state sintering method. We studied the phase composition and microstructure of the ZnO linear resistors, and analysed the mechanism of the effect of La_2O_3 on the electrical properties of ZnO linear resistors.

[#]These authors contributed equally.
*Corresponding author:
Tel : +86-0816-2419203
E-mail: liliangfeng@swust.edu.cn

Experimental and Methods

ZnO linear resistors were fabricated through conventional solid-state sintering method with analytical grade raw materials. The mass compositions was (86.684-*x*) wt.% ZnO+7 wt.% Al_2O_3+5 wt.% MgO+0.6 wt.% TiO_2+0.716 wt.%Y_2O_3+*x* wt.% La_2O_3 (x = 0, 0.25, 0.5, 0.75 or 1). The raw materials were mixed with deionized water in a planetary ball mill at a speed of 356 r/min for 24 h. The mass ratio of powders, water, and zirconia balls was 1:3:3. The resulting slurry was dried at 100 °C for 24 h in an air dry oven. The obtained dry mixture was crashed into powders and prilled with 8 wt.% PVA, followed by aging for 24 h. The prilled powders were pressed into discs with 20 mm in diameter and 3 mm in thickness under the pressure of 10 MPa, and then the discs were sintered for 3 h at 1360 °C. Finally, after a cooling procedure (2 °C/min), the specimens were polished and coated with aluminum electrodes for further electric measurement.

The microstructure of the as-prepared specimens was observed by a scanning electron microscope (Hitachi desktop TM - 4000, Japan), and the grain size was calculated based on the linear intercept method [30]. The elemental distribution of the specimens were determined by an energy dispersive spectrometer (EDS). The crystalline phase and lattice constants of the specimens were characterized by an X-ray diffractometer (XRD, DMAX1400, Japanese physics) using Cu Kα radiation (λ = 0.154 nm).

The *I-V* curves of ZnO linear resistors at 0-4 V were measured by HRMS-800 high temperature insulating material resistivity measurement system. The nonlinear coefficient of was calculated by the following equation [31]:

$$\alpha = \frac{\lg(I_2 / I_1)}{\lg(U_2 / U_1)} \tag{1}$$

where U_1 and U_2 are the voltage values at two different points of an *I-V* curve, I_1 and I_2 are the current values at the voltage of U_1 and U_2 respectively. In this paper, the obtained α is averaged over 10 data points. The resistance-temperature (*R-T*) curves of ZnO linear resistors in the temperature range of 25-300 °C were tested by HRMS-900 high temperature insulating material resistivity measurement system. The resistance-temperature coefficient is calculated by the following equation [32]:

$$\alpha_T = \frac{R - R_0}{(T - T_0)R_0} \tag{2}$$

where T_0 is the initial temperature of the test (25 °C), R_0 is the resistance of the sample at 25 °C, R is the resistance of the sample at temperature T. The calculation is averaged over 10 data points.

Results and Discussion

XRD characterization

Fig. 1 shows XRD patterns of the ZnO linear resistors with different amounts of La_2O_3 additive. The main crystalline phase compositions of the ZnO linear resistors without La_2O_3 are ZnO, $ZnAl_2O_4$, and $MgAl_2O_4$. After the addition of La_2O_3, a diffraction peak with a low intensity appears at 32°-33°, and its intensity increases with the increase of La_2O_3 addition. The phase corresponding to this diffraction peak is La-rich phase [22, 33]. The enlarged XRD patterns in the range of 35-38° shows that the addition of La_2O_3 leads to a leftward shift (towards the small diffraction angle) of the diffraction peak of ZnO, which means the increase of lattice parameters. This is due to the replacement of Zn^{2+} (74 pm) by La^{3+} (106 pm) during sintering. With the increase of La_2O_3 addition, the lattice parameters of

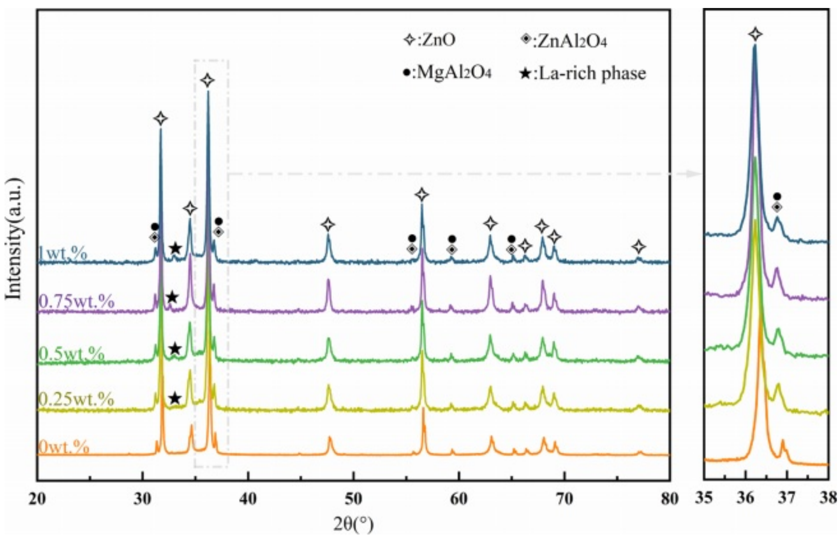

Fig. 1. XRD patterns of the ZnO linear resistors with different amount of La_2O_3.

Table 1. Lattice parameters of ZnO in ZnO linear resistors added different amounts of La_2O_3.

La_2O_3 (wt.%)	Lattice parameters (Å)		c/a
	a=b	c	
0	3.2461	5.1818	1.5963
0.25	3.2542	5.1944	1.5962
0.5	3.2545	5.1976	1.5970
0.75	3.2546	5.1995	1.5976
1	3.2534	5.1924	1.5960

ZnO increase first and then decrease, as shown in Table 1. When the addition of La_2O_3 is 0.75 wt.%, the lattice parameters of ZnO reach the maximum. Further increasing La_2O_3 to 1 wt.% decreases the lattice parameters of ZnO. This may be due to the fact that when too much La_2O_3 is added, it is more likely to segregate at the grain boundaries and resulting in less La^{3+} entering the ZnO lattice.

Bulk density

The bulk density and relative density of the samples with different different amounts of La_2O_3 are shown in Fig. 2. The density of the samples increases with the increase of La_2O_3 addition, and slightly decreases when the addition of La_2O_3 is greater than 0.75 wt.%. When the addition of La_2O_3 is 0.75 wt.%, the bulk density and relative density of the ZnO linear resistors are 5.040 g/cm^3 and 95.27% respectively, which are the maximum values of these samples. The slightly increased density of the samples with the addition of La_2O_3 is because La_2O_3 has the effect of activating the lattice [22]. However, when the La_2O_3 addition is 1 wt.%, the segregation of the La-rich phase at the grain boundaries affects the homogeneity of ZnO [29] and cause the decrease of density.

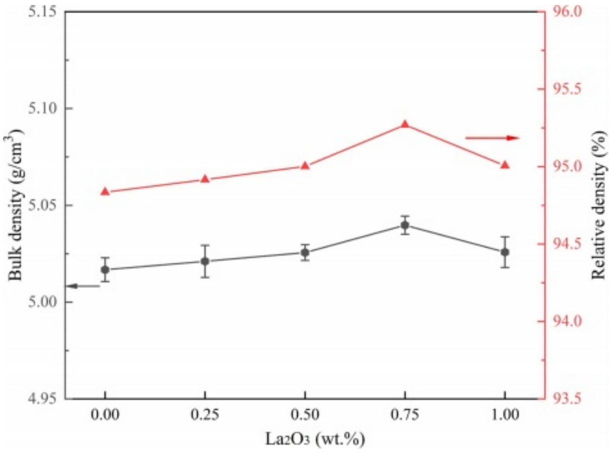

Fig. 2. The bulk density and relative density of ZnO linear resistors with different amount of La_2O_3.

Microstructure characterization

To understand the impact of the La_2O_3 on the microstructure, we observed the morphology of the samples with different amounts of La_2O_3 by SEM, as shown in Fig. 3. Without the addition of La_2O_3, the ZnO grains are irregularly slender in shape. With the increase of La_2O_3 addition, a new phase (bright areas in Fig. 3(c-e)) appeared, which may be La-rich phase that manifested in XRD patterns. Moreover, the ZnO grain size increases with the increase of La_2O_3 addition except the sample with La_2O_3 addition of 0.75 wt.% (as summarized in Table 2). When the addition of La_2O_3 is 0.75 wt.%, the ZnO grain size is significantly refined and uniformly distributed.

During the sintering process, atoms diffuse along the grain boundaries, causing migration of grain boundaries

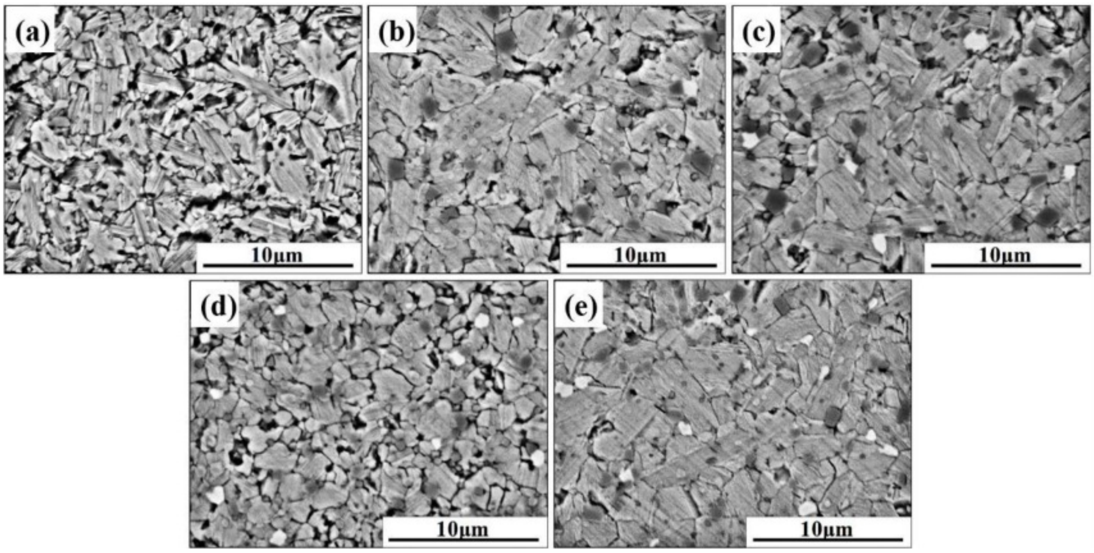

Fig. 3. SEM images of ZnO linear resistors with different amount of La_2O_3. (a) without La_2O_3, (b) 0.25 wt.% La_2O_3, (c) 0.5 wt.% La_2O_3, (d) 0.75 wt.% La_2O_3, and (e) 1 wt.% La_2O_3.

Table 2. Average grain size of ZnO linear resistors with different amounts of La_2O_3.

La_2O_3 (wt.%)	0	0.25	0.5	0.75	1
Average grain sizes (μm)	3.33	3.66	3.75	2.67	3.72

and growth of grains [34, 35]. The migration of grain boundaries is determined by the distribution of the second phase at the grain boundaries and the defects in other regions. The effect of La_2O_3 on the microstructure of ZnO linear resistors is mainly manifested in two ways: (1) La^{3+} distributes at the grain boundaries and activates the migration of grain boundaries, leading to the growth of ZnO grains; (2) La^{3+} enters the lattice of ZnO by substituting Zn^{2+} [29], which inhibit the migration of grain boundaries and the growth of grains. When the amount of La_2O_3 is small, La^{3+} ions mainly distribute at the grain boundaries, which results in the increase of grain size. However, with the increase of La_2O_3, more La^{3+} ions enter the lattice of ZnO and

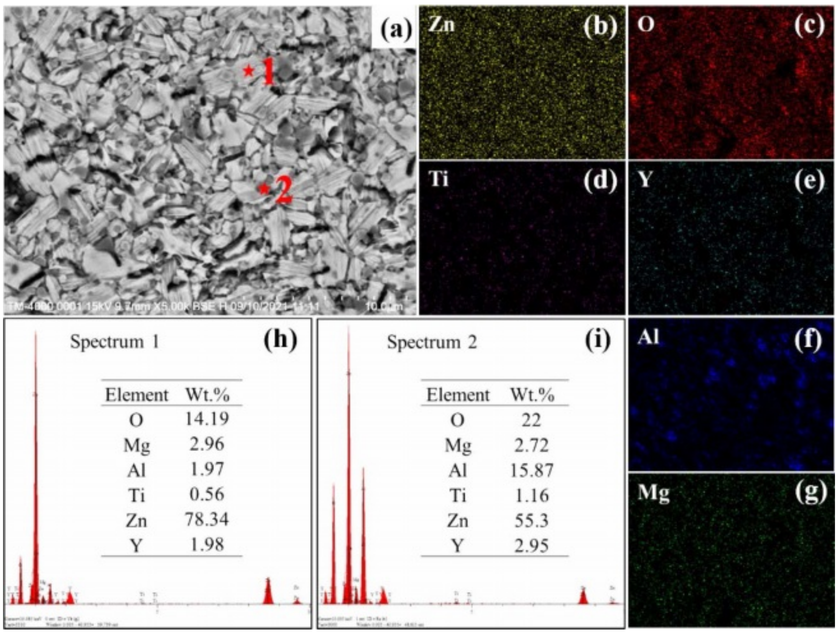

Fig. 4. EDS characterization of ZnO linear resistor without addition of La_2O_3. (a) SEM image, (b)-(g) element mappings of Zn, O, Ti, Y, Al, and Mg. (h) and (i) show the energy dispersive spectra of the ZnO grain (position 1) and spinel phase (position 2), respectively.

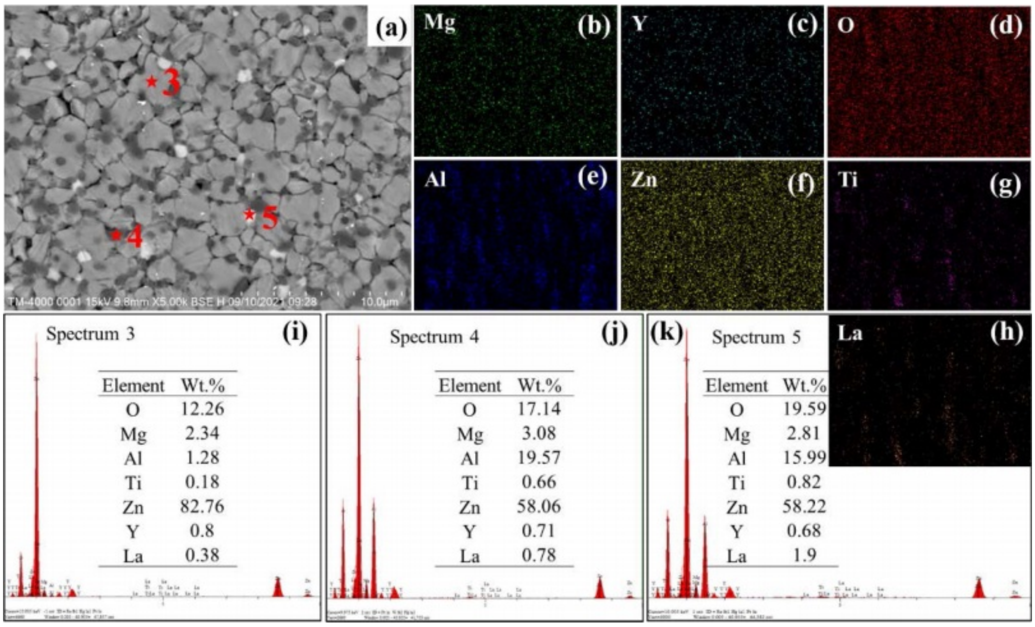

Fig. 5. EDS characterization of ZnO linear resistor with 0.75 wt.% La_2O_3. (a) SEM image, (b)-(h) element mappings of Mg, Y, O, Al, Zn, Ti, and La. (i)-(k) show the energy dispersive spectra of the ZnO grain (position 3), spinel phase (position 4), and La-rich phase (position 5), respectively.

inhibit the growth of grains.

To further determine the phase composition of the ZnO linear resistors, we performed EDS measurements. Fig. 4 and Fig. 5 show the EDS results of ZnO linear resistors without and with 0.75 wt.% La_2O_3, respectively. According to the element mappings and element ratios results, the sample without addition of La_2O_3 is mainly composed of ZnO (light grey areas) and spinel phase (dark grey areas). In the sample with 0.75 wt.% La_2O_3, La element is mainly distributed at the grain boundaries and formed the La-rich phase (bright areas). In addition, the aggregation of Ti element at the grain boundaries in the sample with 0.75 wt.% La_2O_3 is significantly enhanced compared with the sample without addition of La_2O_3. Ti element can enter the ZnO lattice and promote the growth of grain [16]. The aggregation of Ti element at the grain boundaries indicate that there is less Ti in ZnO lattice, which may be a reason that cause the refinement of ZnO grains in the sample with 0.75 wt.% La_2O_3.

Electrical properties

It is critical to know the electrical properties of La_2O_3 doped ZnO linear resistors, such as the resistivity, resistance-temperature coefficient, and nonlinear coefficient of the samples. Fig. 6 shows the resistance and resistivity of ZnO linear resistors with different amounts of La_2O_3. The resistance and resistivity of ZnO linear resistors decrease significantly with the increase of La_2O_3. The resistance (resistivity) values of the sample without addition of La_2O_3 is 16.12 Ω (137.18 Ω·cm), and the resistance (resistivity) values of the sample with 1 wt.% La_2O_3 is decreased to 3.95 Ω (32.76 Ω·cm). The resistance of ZnO linear resistors is determined by both the low resistance ZnO grain and the high resistance grain boundary phase. The addition of La_2O_3 not only affects the grain boundaries, but also reduces the resistance of ZnO grains because La^{3+} enter the lattice of ZnO can increase the concentration of free electrons [29]. As a result, the resistance and resistivity of ZnO linear resistors decreases with the addition of La_2O_3.

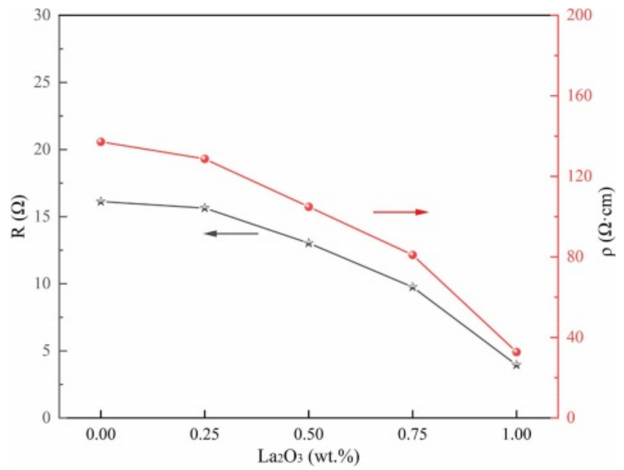

Fig. 6. Resistance and resistivity of ZnO linear resistors with different amount of La_2O_3.

The resistance-temperature coefficients of the ZnO linear resistors are shown in Fig. 7. The absolute values of the ZnO linear resistors with different amounts of La_2O_3 were reduced to smaller than 10^{-3}/°C, which indicate that the addition of La_2O_3 improves the temperature stability of the ZnO linear resistors noticeably. When the addition of La_2O_3 is 0.5 wt.%, the sample has the best temperature stable performance with a resistance-temperature coefficient of 0.21×10^{-3}/°C. The improvement of the temperature stable performance of ZnO linear resistors is because the added La_2O_3 influenced the grain boundaries and promoted the conductance of ZnO.

Fig. 8 shows the nonlinear coefficient of ZnO linear resistors with different amounts of La_2O_3. The addition of La_2O_3 increases the nonlinear coefficient of the samples except the sample with 0.5 wt.% La_2O_3. We further analysed the temperature dependent resistivity according to the thermally activated conduction mechanism

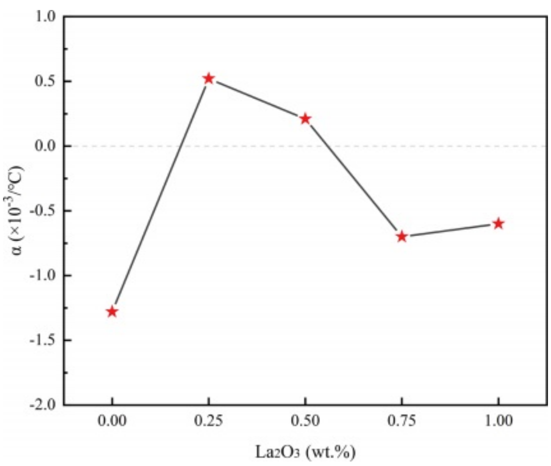

Fig. 7. Resistance-temperature coefficient of ZnO linear resistors with different amount of La_2O_3.

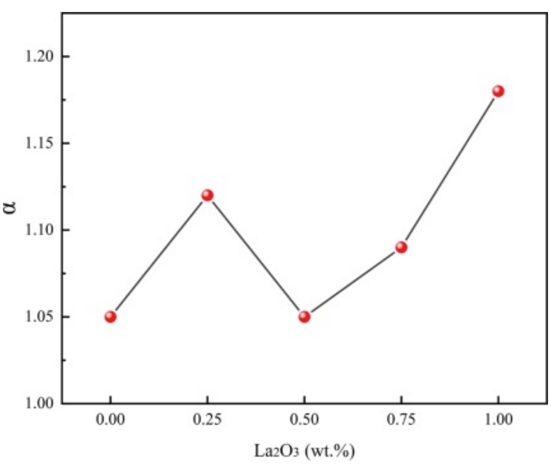

Fig. 8. Nonlinear coefficient of ZnO linear resistors with different amount of La_2O_3.

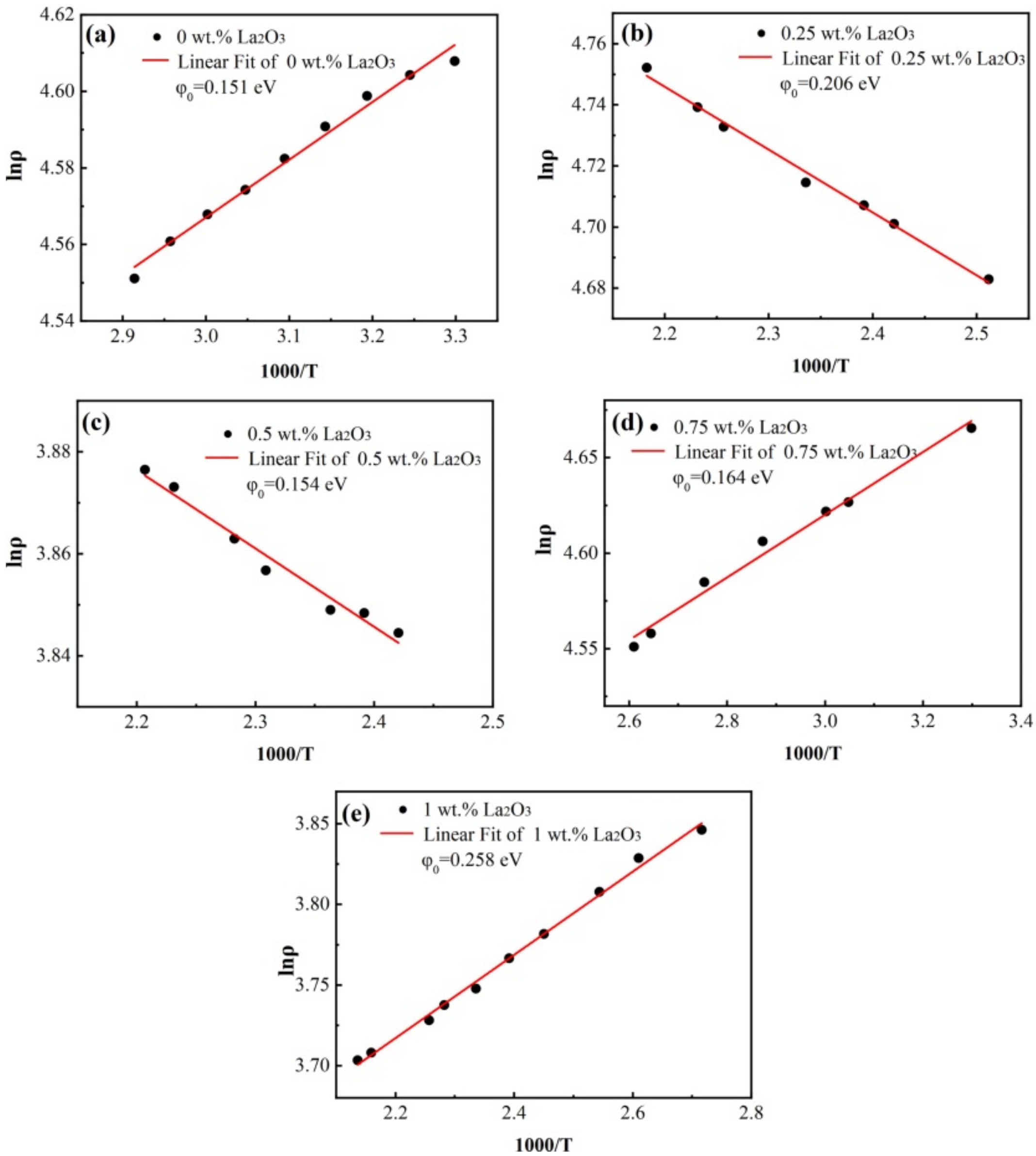

Fig. 9. Arrehenius plots of the temperature dependent resistivity of ZnO linear resistors with different amount of La_2O_3. (a) without La_2O_3, (b) 0.25 wt.% La_2O_3, (c) 0.5 wt.% La_2O_3, (d) 0.75 wt.% La_2O_3, and (e) 1 wt.% La_2O_3.

because the electrical transport in semiconductor ceramics is thermally activated. The resistivity of ZnO linear resistors can be expressed as [17, 22]

$$\rho = \rho_0 e^{(\varphi_0/kT)} \tag{3}$$

where ρ is the resistivity of the sample, ρ_0 is the resistivity of the sample as the temperature tends to infinity; φ_0 is the height of the grain boundary potential barrier (equal to value of the activation energy), k is the Boltzmann constant, and T is the absolute temperature. The Arrhenius plots of the temperature dependent resistivity of ZnO linear resistors are shown in Fig. 9. We linearly fitted the relationship between lnρ and 1000/T and obtained the height of the grain boundary potential barrier by calculating the slops. Here, all the coefficient of determination (R^2) are greater than 0.98, indicating that the electrical transport in ZnO linear resistors matches the thermally activated conduction mechanism well. The addition of La_2O_3 increases φ_0 obviously except the sample with 0.5 wt.% La_2O_3, which is consistent with the trend of nonlinear coefficient. This indicate that the nonlinearly electrical characteristic of La_2O_3 doped ZnO linear resistors is determined by the grain boundary potential barrier, which is adjusted by the addition of La_2O_3.

The potential barrier height φ_0 is expressed by the following equation [17, 22]:

$$\varphi_0 = \frac{e^2 N_s^2}{2 N_d \varepsilon_0 \varepsilon} \tag{4}$$

where e is the elementary charge, N_S is the density of interfacial state, N_d is the donor density, ε is relative dielectric constant, and ε_0 is the vacuum dielectric constant. When La_2O_3 is added into ZnO linear resistors, some of the La^{3+} ions enter ZnO lattice to increase the donor density N_d and decrease φ_0; the other La^{3+} ions distribute at the grain boundaries to generate La-rich phase, which increase the density of interfacial state N_S and thus increase φ_0. Because ionic radius of La^{3+} (106 pm) is much greater than that of Zn^{2+} (74 pm), the amount of La^{3+} ions that entering ZnO lattice is limited and most of the La^{3+} ions are distribute at the grain boundaries to generate La-rich phase. As a result, the height of the grain boundary potential barrier is increased and the nonlinearity of the *I-V* curves also increased.

Due to the complicated components of La_2O_3 doped ZnO linear resistors, all the main crystalline phases, including ZnO, spinel phase, and La-rich phase, can affect the grain boundary potential barrier and charge transport, which makes the factors that affect their electrical conductance quite complex. Thus, more researches are needed in the future to better understand the resistance-temperature characteristic and *I-V* characteristic.

Conclusions

$ZnO-MgO-Al_2O_3-TiO_2-Y_2O_3$ linear resistors doped with different amount of doping were prepared through the conventional solid-state sintering method, and the effect of La_2O_3 on the microstructure and electrical properties of these resistors was investigated. The addition of La_2O_3 increased the lattice constant of ZnO due the substitution of La^{3+} for Zn^{2+}, and generated La-rich phase at the grain boundaries due to the reaction between La_2O_3 and the components of ZnO linear resistor. As a result, the addition of La_2O_3 modulated the grain boundary potential barrier and improved the temperature stability of ZnO linear resistors. The sample with 0.5 wt.% La_2O_3 showed excellent resistance-temperature characteristic with an resistance-temperature coefficient of 0.21×10^{-3}/°C, and good linear *I-V* characteristic with an nonlinear coefficient of 1.05. This work indicates that the doping of rare earth oxides may modulate the microstructure and hence benefits the performance improvement of ZnO based linear resistors.

Acknowledgements

This study was sponsored by the National Natural Science Foundation of China (No. 11405140), the Scientific Research Fund of Sichuan Provincial Education Department (No. 17ZA0395) and the Longshan Academic Talent Research Supporting Program of SWUST (No. 18LZX609, 18LZX679).

Declarations:

Conflict of interest: the authors declare that there are no conflicts of interest.

References

1. J. Wang, J. Wang, J. Ding, Y Wei, and J. Zhang, Solid State Sci. 127 (2022) 106860.
2. D.B. Lakshmi, R.S. Rajendran, J. Suthakorn, and B.M. Pillai, J. Ceram. Process. Res. 23 (2022) 878-883.
3. P. Fan, D. Zhang, Y. Wu, J. Yu, and T.P. Russell, Adv. Funct. Mater. 30 (2020) 2002932.
4. A.L. Nikolaev, M.A. Kazmina, N.V. Lyanguzov, K.G. Abdulvakhidov, and E.M. Kaidashev, J. Adv. Dielectr. 12 (2022) 2160020.
5. H. Parka, H. Ahnb, S.H. Kimc, and D.J. Kima, J. Ceram. Process. Res. 17 (2016) 632-636.
6. S. Park, G.J. Sun, and C. Lee, J. Ceram. Process. Res. 16 (2015) 367-371.
7. S. Fu, W. Wang, L. Qian, Q. Li, Z. Lu, J. Shen, C. Song, F. Zeng, and F. Pan, IEEE Electr. Device L. 40 (2018) 103-106.
8. B. Bayraktaroglu, K. Leedy, and R. Neidhard, IEEE Electr. Device L. 30 (2009) 946-948.
9. S. Krishnamoorthy, and A.A. Iliadis, Solid State Electron. 52 (2008) 1710-1716.
10. S. Goktas and A. Goktas, J. Alloy. Compd. 863 (2021) 158734.
11. F. Song, Y. Sun, and P. Rao, J. Ceram. Process. Res. 22 (2021) 521-526.
12. M. Ji and Y.I. Lee, J. Ceram. Process. Res. 22 (2021) 386-393.
13. L. Levinson and H. Philipp, IEEE Trans. Parts, Hybrids, Packag. 13 (1977) 338-343.
14. S.H. Lee, C.K. Sohn, A. Djafar, M.T. Cho, and J.R. Yoon, J. Ceram. Process. Res. 20 (2019) 164-168.
15. Z. Cheng, Z. Hou, T. Wu, Y. Wang, R. Li, Y. Lin, J. Li, S. Li, and K. Wu, J. Appl. Phys. 133 (2023) 054101.
16. J. Zhu, Y. Zhou, H. Yang, and F. Wang, J. Mater. Sci: Mater. Electron. 23 (2012) 445-450.
17. J. Liu, X. Luo, and W. Cao, J. Alloy. Compd. 946 (2023) 169445.
18. Y. Luo, K. He, R. H. Yu, J. P. Qi, H. M. Yuan, J. Xie, and D. Xu, Mater. Res. Innovations. 18 (2014) S4-639.
19. J. Zhu, Q. Liu, J. Wang, Y. Zhou, W. Ye, and F. Wang, J. Mater. Sci: Mater. Electron. 27 (2016) 818-824.
20. J. Zhu, Q. Liu, J. Wang, Y. Zhou, W. Ye, and F. Wang, J. Mater. Sci: Mater. Electron. 25 (2014) 2273-2278.
21. J. Zhu, Q. Liu, J. Wang, F. Wang, H. Yang, and L. Wang, J. Mater. Sci: Mater. Electron. 27 (2016) 5729-5734.
22. J. Liu, J. Chen, R. Zhang, J. Su, Y. Qiao, X. Xie, and W. Cao, J. Alloy. Compd. 866 (2021) 158855.
23. M. Chen, Q. Liu, J. Zhu, and F. Wang, J. Alloy. Compd. 750 (2018) 213-219.
24. T. Shirakawa, M. Miyayama, Y. Nakamura, and H. Yanagida, J. Mater. Sci. Lett. 10 (1991) 381-383.
25. J. Zhu, J. Wang, Y. Zhou, and F. Wang, J. Mater. Sci: Mater. Electron. 25 (2014) 791-796.
26. J. Yin, C. Huang, Z. Tang, and C. Shen, J. Electron. Mater. 49 (2020) 4864-4871.
27. M. Shoji, S. Tanaka, S. Shirakawa, and S. Yamada, J. Ceram. Soc. Jpn. 108 (2000) 89-93.
28. N. Obradovic, M. Mitric, M.V. Nikolic, D. Minic, N. Mitrovic, and M.N. Ristic, J. Alloys Compd. 471 (2009)

272-277.
29. J. Wang, J. Zhu, Y. Zhou, and F. Wang, J. Mater. Sci: Mater. Electron. 25 (2014) 3301-3307.
30. J.C. Wurst and J.A. Nelson, J. Am. Ceram. Soc. 55 (1972) 109.
31. R. Einzinger, Annu. Rev. Mater. Sci. 17 (1987) 299-321.
32. F. Zandman and J. Szwarc, J. Vishay Precision Group, Tech. Rep. 108 (2013) 55.
33. X. Dong, Y. Gan, Y. Wang, S. Peng, and L. Dong, J. Alloy. Compd. 581 (2013) 52-55.
34. M. Inada, Jpn. J. Appl. Phys. 17 (1978) 1-10.
35. J. Lu, L. Li, B. Zhou, X. Ma, and H. Yan, ECS J. Solid State Sci. 10 (2021) 103014.